Applied Sig Process (1998)5:40–48

Applied Signal Processing

Studying the Interaction Between Brain Structures via Directed Coherence and Granger Causality

L. A. Baccalá[1], K. Sameshima[2,3], G. Ballester[3], A. C. Do Valle[3] and C. Timo-Iaria[3]

[1]Electronics Engineering Department, Escola Politécnical, University of São Paulo, Brazil; [2]Discipline of Medical Informatics, University of São Paulo, Brazil; and [3]Functional Neurosurgery Lab., School of Medicine, University of São Paulo, Brazil

This paper reviews the recently proposed method of directed coherence and the related concept of Granger causality testing which jointly allow the direction of information flow between multiple brain structures to be deduced in a statistically significant manner. Through spectral factorisation using vector autoregressive models and an allied feedback-based system-theoretic structure interpretation, these methods permit tracking alterations in the connectivity of the functioning brain of active animals, thereby opening a new set of possibilities for neural signal analysis. Illustrative examples are provided using signals from the cortex and hippocampus of both sleeping and active rats where noticeable shifts in the direction of information flow take place according to sleep state and due to the influence of external stimuli.

Keywords: Brain rhythmic oscillation; Desynchronised sleep; Directed coherence; Granger causality; Information flow

1. Introduction

For a long time, anatomical (i.e. structural) data obtained from animal dissection remained the only source of information on how brain areas interrelate. In the last six decades, actual physiological functional data became available through the analysis of neuroelectric signals collected from living animals. By far, the most popular signal analysis tools in brain research today are variants of spectrum-based correlation/coherence function analysis [1–4] whereby the relationships between the simultaneous neural activity of distinct brain areas, represented by time series $x(t)$ and $y(t)$, are probed via statistical tests over hypothetical linear signal mappings T (filters)

$$y(t) = T\,x(t) \tag{1}$$

The adequacy of this model is usually asserted by means of the classical coherence function

$$C_{xy}(f) = \frac{S_{xy}(f)}{\sqrt{S_x(f)S_y(f)}} \tag{2}$$

where $S_x(f)$ and $S_y(f)$ are the power spectral densities at the input and at the output of T, respectively, and $S_{xy}(f)$ is the corresponding cross-spectral density. Since T is usually invertible,

$$x(t) = T^{-1}y(t) \tag{3}$$

holds as well and its validity is also verifiable through Eq. (2), whereby the choice of using $x(t)$ or $y(t)$ as the model input is completely arbitrary.

Some developments in multivariate time series analysis have opened a whole new perspective of description through the concept of Granger causality [5]. Born out of econometrics and named after its proponent to distinguish it from other and more general issues involving cause and effect in philosophy [6] and in system theory, this concept enables us to draw a dynamical picture of the functional interactions between structures in the active brain.

By contrast with ordinary coherence analysis,

Correspondence and offprint requests to: L.A. Baccalá, Electronics Engineering Department, Escola Politécnica, University of São Paulo, Av. Prof. Luciano Gualberto, Trav. 3, #158, CEP 05508-900, São Paulo, SP, Brazil. Email: baccala@lcs.poli.usp.br.

Granger causality lacks symmetry with respect to swaps between $x(t)$ and $y(t)$. This feature turns out to be essential in pointing the direction of information flow.

There are many possible definitions of Granger causality [5–8]. Roughly speaking, $x(t)$ Granger-causes $y(t)$ if substantial improvements occur in predicting $y(t)$ by also taking the past of $x(t)$ into account. Also noteworthy for neural structure characterisation is the intimate relationship between this concept and the 'issue' of feedback detection [9].

To a large extent the signal processing community, with the exception of applied econometricians, remains largely unaware of Granger causality and its potential uses. For this reason, Section 2 contains a brief review of the concept and elaborates some of its consequences together with methods of inference for its existence. Section 3 is devoted to the consideration of applications in neurobiology; this is followed by a discussion of future perspectives and open issues in Section 4. For ease of reference, a version of the Granger causality test performed in the examples is described in the Appendix.

2. Background

Even though the method applies to many simultaneous time series, for simplicity we consider just two time series y and x which one may represent by the filtering of unobservable time series w_y, w_x assumed to be zero mean i.i.d. sequences of suitable statistics:

$$\begin{bmatrix} y \\ x \end{bmatrix} = \mathbf{H} \begin{bmatrix} w_y \\ w_x \end{bmatrix} = \begin{bmatrix} H_{yy} & H_{yx} \\ H_{xy} & H_{xx} \end{bmatrix} \begin{bmatrix} w_y \\ w_x \end{bmatrix} \tag{4}$$

where if H_{ij} are linear operators, Eq. (4) is called the prediction error filter representation of the vector process $[y \quad x]^T$ [10]. By using general operators, H_{ij}, extension to the case of N time series becomes immediate. For instance, if H_{ij} stand for matrices, x and y can be viewed themselves as vector processes. Also for simplicity, operator invertibility is henceforth assumed.

Obviously if $\mathbf{H}$ is triangular, it is easy to see that w_y and w_x affect x and y asymmetrically, leaving more room for dynamical variability in one of the series than in the other. To see this, let us express y as a function of x,

$$y = H_{yx} H_{xx}^{-1} x + (H_{yy} - H_{yx} H_{xx}^{-1} H_{xy})\, w_y \tag{5}$$

where, if $H_{yx} \equiv 0$, x has no bearing on y as

$$y = H_{yy}\, w_y \tag{6}$$

Despite this, we may still represent x as a function of y:

$$x = H_{xy} H_{yy}^{-1} y + (H_{xx} - H_{xy} H_{yy}^{-1} H_{yx})\, w_x \tag{7}$$

or

$$x = H_{xy} H_{yy}^{-1} y + H_{xx}\, w_x \tag{8}$$

To capture this asymmetry we may say that x Granger-causes y if and only if $H_{yx} \neq 0$ in Eq. (5).

This relation is directional in the sense that x can 'cause' y, without y 'causing' x, provided that $H_{xy} \equiv 0$ and $H_{yx} \neq 0$. In other words, no information flows from y to x or equivalently, given signal propagation delays, as we argue subsequently there is no feedback from y onto x. To realise this, draw a block diagram representation corresponding to Eqs (5) and (7) [11], whose general form is

$$\begin{bmatrix} y \\ x \end{bmatrix} = \begin{bmatrix} 0 & G_{yx} \\ G_{xy} & 0 \end{bmatrix} \begin{bmatrix} y \\ x \end{bmatrix} + \begin{bmatrix} G_{yy} & 0 \\ 0 & G_{xx} \end{bmatrix} \begin{bmatrix} \varepsilon_y \\ \varepsilon_x \end{bmatrix} \tag{9}$$

which, upon elimination of the variables, gives

$$\begin{bmatrix} y \\ x \end{bmatrix} = \begin{bmatrix} I & -G_{yx} \\ -G_{xy} & I \end{bmatrix}^{-1} \begin{bmatrix} G_{yy} & 0 \\ 0 & G_{xx} \end{bmatrix} \begin{bmatrix} \varepsilon_y \\ \varepsilon_x \end{bmatrix} \tag{10}$$

or

$$\begin{bmatrix} H_{yy} & H_{yx} \\ H_{xy} & H_{xx} \end{bmatrix} = \begin{bmatrix} (I - G_{yx}G_{xy})^{-1} G_{yy} & (I - G_{yx}G_{xy})^{-1} G_{yx}G_{xx} \\ (I - G_{xy}G_{yx})^{-1} G_{xy}G_{yy} & (I - G_{xy}G_{yx})^{-1} G_{xx} \end{bmatrix} \tag{11}$$

which leads to $G_{xy} = 0$ if $H_{xy} = 0$ representing lack of feedback from y to x. One may show also the validity of the converse, making lack of feedback synonymous with absence of Granger causality [12], provided some mild regularity conditions that guarantee invertibility of the operators involved (like the lack of instantaneous signal propagation in the feedback loop) [12,13].

Remark 1. Generalisation to N time series is immediate. If $\tilde{H}_{ij}$ is an element of the generalised $\mathbf{H}^{-1}$ then

$$G_{ij} = \frac{\tilde{H}_{ij}}{\tilde{H}_{ii}} \tag{12}$$

and

$$G_{ij} = -\hat{H}_{ii}^{-1}\hat{H}_{ij} \tag{13}$$

Thus Granger causality analysis requires the *a priori* definition of the time series prediction models (usually parametric) to be used. Because of its simplicity and low computational complexity, most authors restrict themselves to linear models. This choice is attractive because the spectral representation $S(f)$ of $[y\ x]^T$ can be factored uniquely as

$$S(f) = \begin{bmatrix} H_{yy}(f) & H_{yx}(f) \\ H_{xy}(f) & H_{xx}(f) \end{bmatrix} \Sigma \begin{bmatrix} H_{yy}(f) & H_{yx}(f) \\ H_{xy}(f) & H_{xx}(f) \end{bmatrix}^H \tag{14}$$

where

$$\Sigma = \begin{bmatrix} \sigma_{yy}^2 & \sigma_{yx} \\ \sigma_{xy} & \sigma_{xx}^2 \end{bmatrix}$$

is the cross-covariance matrix between w_y and w_x, and $H_{ii}(f)$ represent minimum phase versions of H_{ii} filters in Eq. (4) [12,13], affording practical computational means that generalise immediately to $N > 2$.

A particularly convenient way to compute $H_{ii}(f)$ is through vector autoregressive (VAR) model fitting of the form

$$\begin{bmatrix} y(t) \\ x(t) \end{bmatrix} = \sum_{i=1}^{p} \mathbf{A}_i \begin{bmatrix} y(t-i) \\ x(t-i) \end{bmatrix} + \begin{bmatrix} \varepsilon_y(t) \\ \varepsilon_x(t) \end{bmatrix} \tag{15}$$

where the

$$\mathbf{A}_i = \begin{bmatrix} a_{11}(i) & a_{12}(i) \\ a_{21}(i) & a_{22}(i) \end{bmatrix}$$

are matrices of constant coefficients, leading directly to Eq. (4) by using the z-transform in Eq. (15) and rewriting it as

$$\mathbf{H}(z)\big|_{z=e^{i2\pi f}} = \left(\mathbf{I} - \sum_{i=1}^{p} \mathbf{A}_i z^{-i}\right)^{-1}\Bigg|_{z=e^{i2\pi f}} = \begin{bmatrix} H_{yy}(f) & H_{yx}(f) \\ H_{xy}(f) & H_{xx}(f) \end{bmatrix} \tag{16}$$

Remark 2. There are several estimators for $\mathbf{A}_i$ and criteria for the optimal model order p selection [14–17]. In the illustrations that follow in Section 3, the Nutall–Strand algorithm was used in the computations together with the AIC (Akaike information criterion) for choice of optimal model order [14].

Remark 3. For N time series the feedback representation is easy to express in terms of

$$A_{ij}(z) = \sum_{k=1}^{p} a_{ij}(k) z^{-k} \tag{17}$$

as

$$G_{ii}(z) = \frac{1}{1 - A_{ii}(z)} \tag{18}$$

and, for $i \neq j$,

$$G_{ij}(z) = \frac{A_{ij}(z)}{1 - A_{ii}(z)} \tag{19}$$

From these results, lack of causality from j to i can be measured by either one of three conditions:

$$G_{ij}(z) = \hat{H}_{ij}(z) = A_{ij}(z) \equiv 0 \tag{20}$$

The testability of the condition $a_{ij}(k) = 0$ leads directly to a test for Granger causality. Concisely, lack of Granger causality from j to i cannot be rejected if a suitably weighted linear combination of $a_{ij}(k)$ is significantly different from zero as measured by a χ^2 distribution whose number of degrees of freedom equal the number of linear constraints $a_{ij}(k) = 0$ [7]. The weights over $a_{ij}(k)$ involve the covariance matrices of the time series and of their prediction errors. This type of test is not only convenient in its matrix formulation (see Appendix) but also has superior performance among many other possible test alternatives [18].

Remark 4. In an alternative formalisation of Granger causality [8], the operator G_{yx} must be expressed as

$$G_{yx}(z) = \sum_{i=1} g_{yx}(i) z^{-i}$$

to ensure exploratory inference of the exclusive effect of the past of $x(t)$ on $y(t)$. This imposes lack of instantaneous feedback between time series which is a precondition for the validity of Eq. (14) [12,13]. Thus, the factors H_{ij} which depend on G_{ij} only display information about dependencies of one series on the past of the other series. As a matter of fact, dependency, mainly correlation, of the present of a time series on the present of another time series can be investigated using Σ, where inability to statistically reject $\sigma_{yx} = 0$ indicates the possibility for substantial improvement in the prediction of $y(t)$ by considering the present of $x(t)$ in addition to its past. Whenever $\sigma_{yx} \neq 0$, it is usual to speak of *instantaneous causality* between the time series [7]. This type of causality is, alas, symmetric (like classical coherence, Eq. (2)) because $\sigma_{yx} = \sigma_{xy}$ and may indicate the presence of external signal

sources influencing $x(t)$ and $y(t)$ simultaneously. Further modelling to explain $\sigma_{vv} = 0$ in terms of additional noise sources requires additional *ad hoc* assumptions that violate the uniqueness of the spectral representation (Eq. (14)) as in [19].

Despite the ability to probe for Granger causality directly, some researchers have considered the use of an alternative frequency domain measure of causality called the *directed coherence* (a terminology due to [19]) from series j to series i and definable in a form generalisable to N time series as [11]

$$\gamma_{ij}(f) = \frac{\sigma_{ij}H_{ij}(f)}{\sqrt{S_i(f)}} \tag{21}$$

where

$$S_i(f) = \sum_{j=1}^{N} \sigma_{ij}^2 |H_{ij}(f)|^2 \tag{22}$$

is the power spectral density of the ith series so that $|\gamma_{ij}(f)|^2$ represents the fraction of the power in the ith series due to the past of the jth series. Hence follow

$$0 \leq |\gamma_{ij}(f)| \leq 1 \tag{23}$$

and

$$\sum_{j=1}^{N} |\gamma_{ij}(f)|^2 = 1 \tag{24}$$

If, for instance, Eq. (21) provides an interesting frequency-dependent picture of signal flow, its asymptotic statistical properties remain theoretically unknown with precision and only some extensive Monte Carlo simulations have provided a practical limit of $|\gamma_{ij}(f)|^2 < 0.1$ as claimed evidence for lack of causality at a given frequency [11].

Remark 5. For the bivariate case, $\gamma_{ij}(f)$ is closely related to a causality test proposed by Geweke [20] that is essentially equivalent to the one considered previously and whose alternative statistic $F_{X\to Y}$ can be decomposed in the frequency domain as

$$F^{X\to Y} = \frac{1}{2\pi} \int_{-\pi}^{\pi} f_{X\to Y}(\lambda) d\lambda \tag{25}$$

where one may show that

$$e^{-f_{X\to Y}(\lambda)} + |\gamma_{yx}(\lambda)|^2 = 1 \tag{26}$$

Remark 6. The so-called method of directed transfer function (DTF) [21,22] differs from the above formulation solely by using $\sigma_{ij} = 1$ in Eqs (21) and (22), which precludes interpretation of the resulting quantity as in terms of signal power fractions.

In neurobiology, knowledge of signal frequency distributions is often physiologically significant (in identifying α-rhythms for instance) so that testing for causality by checking $a_{ij}(k) = 0$ together with plotting $|\gamma_{ij}(f)|^2$ provide complementary information, one with regard to causality significance and the other with regard to frequency distribution. Thus whenever Granger causality cannot be dispelled, $|\gamma_{ij}(f)|^2$ provides information about the relative importance of the frequencies involved in the phenomenon. Our signal processing protocols are illustrated in the next section.

3. Methods and Illustrations

To illustrate the use of these ideas and their significance for neurobiology, we selected two samples of multi-channel traces of local field potentials recorded from cortical and subcortical brain structures of rats in sleep and in wakefulness via chronically implanted bipolar electrodes (Figs 1 and 3).

Figure 1 presents 60 s traces acquired during desynchronised sleep, in many ways equivalent to human REM sleep, in which the rat presented rhythmic oscillations of brain electrical activity around 8 Hz in the hippocampal fields CA1 and CA3, and two cortical Krieg's areas, A10 and A3 [23]. The muscular electrical activities related to rostrum and eye movements were also simultaneously recorded. In analogy to human sleep, it is believed that other species, including rats, also experience dreaming during desynchronised sleep, which can be evidenced by the phasic muscle activity of rostrum and eye movements that characterise a dreaming episode. In Fig. 1, four such episodes are present, starting at approximately 5, 15, 28 and 37 s; they are accompanied or preceded by a slight transient increase in the oscillatory frequency. This fluctuation of oscillatory frequency with such episodes can be appreciated by looking at the peak of classical coherence function in Fig. 2c.

To investigate the causal relationships between these regions, VAR models were fitted to 2 s windows with 50% overlapping among adjacent segments; this choice has being made to reduce the effect of signal nonstationarity. The resulting time–frequency evolution for $\gamma_{CA1,CA3}(f)$ (high in the vicinity of 8 Hz) and $\gamma_{CA3,CA1}(f)$ is illustrated via grey-scale plots of Figs 2(a) and 2(b). Together these results suggest a directionality in information

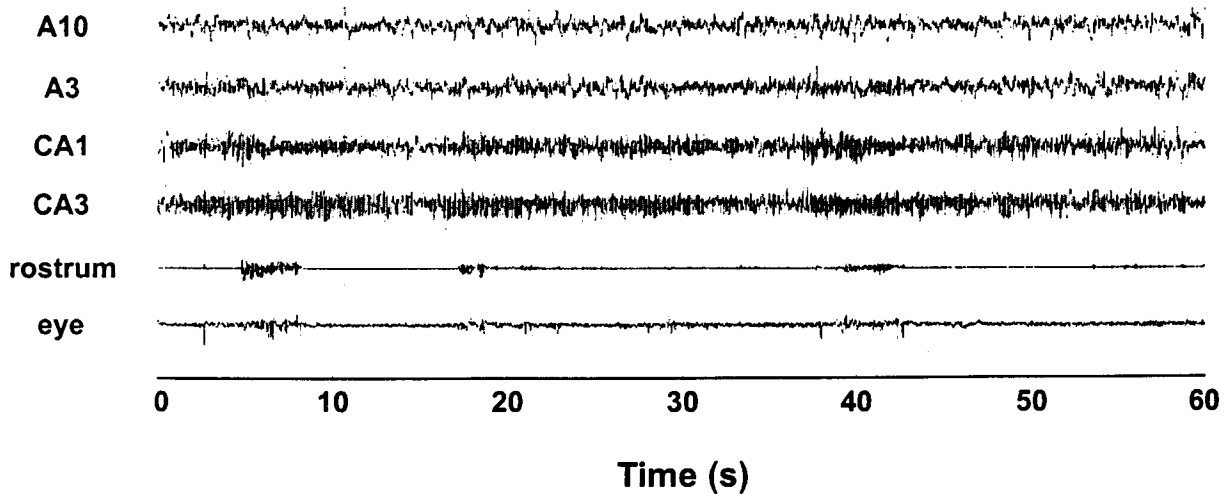

Fig. 1. Local potential field recordings sampled at 256 Hz of a sleeping rat's hippocampal areas CA1 and CA3 and cortical areas A3 and A10. together with the simultaneous electromyograms from rostrum and eye muscles.

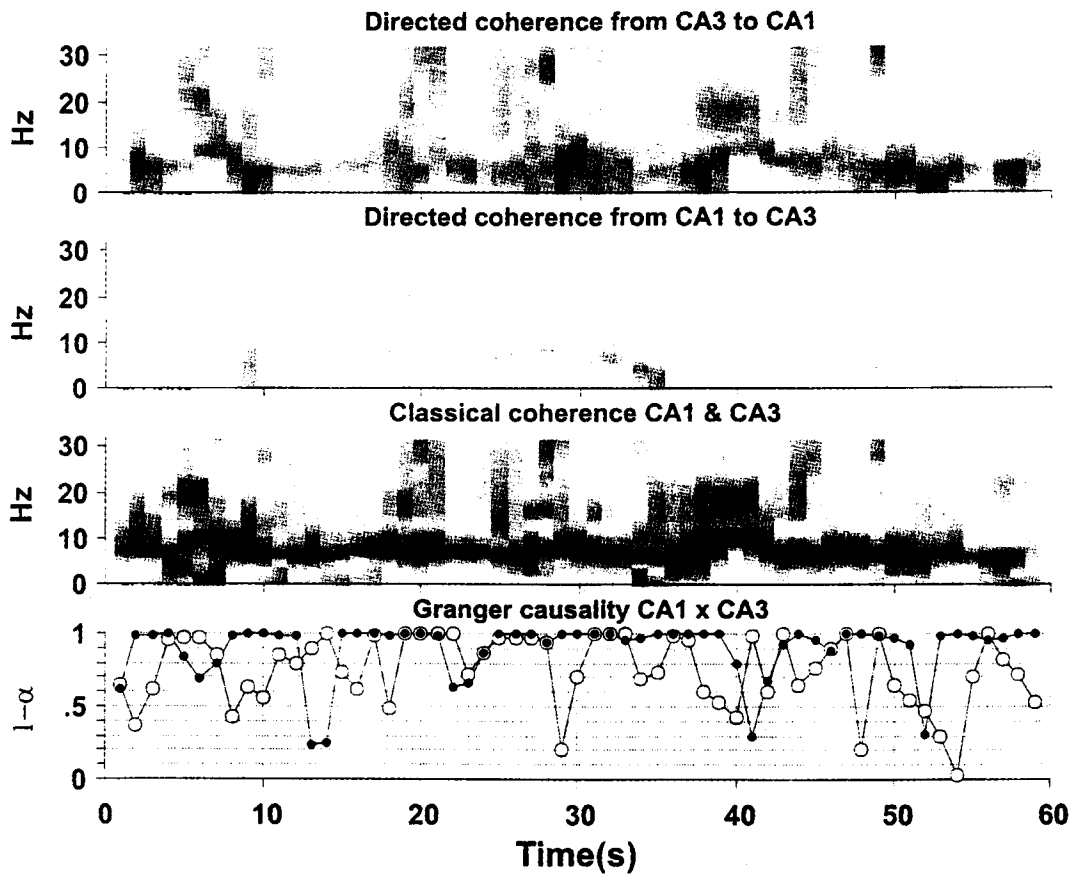

Fig. 2. Comparison of the time–frequency evolution of the directed coherences (**a**) and (**b**) between CA1 and CA3 from Fig. 1 with the corresponding classical coherence (**c**). Figure 2d displays the corresponding results of the Granger causality test in terms of the lower probability tail $1-\alpha$ of the value of the statistic λ_w (see Appendix) for each 2 signal segment used in the computations through joint VAR modelling of all. $N=4$. brain signals in Fig. 1. The symbol ● represents the result of the effect of CA3 on CA1. while C stands for the opposite direction.

flow from CA3 to CA1 that is confirmed in Fig. 2(d) which displays the temporal evolution of the level of significance $(1-\alpha)$ of the Granger causality test statistic λ_{∞} (see Appendix). It is interesting to note that CA3's influence over CA1 is easy to explain on the basis of known direct neuroanatomical projections, whereas signal bidirectionality may be explained by long-loop feedback involving cortex and medial septum and by more recently described diffuse connection from CA1 to CA3, which deserves further study of its functional significance (for more detail about the hippocampus see [24]).

In the Granger causality plot, Fig. 2(d), CA3 is causal onto CA1 (•), whenever $(1-\alpha)>0.95$. Accordingly we observe episodes of information directionality switches that are related to rostrum movements. This fact is not evident through the inspection of directed coherence plots (Figs 2a and 2(b)) because directed coherence from CA3 to CA1, Fig. 2(a), is much stronger and evident than from CA1 to CA3, Fig. 2(b).

In rodents, rhythmic neuroelectric activity in this same frequency range is also observed during active exploratory behaviour. Figure 3 shows a recording from cortex (A3, A10), hippocampus (CA1), and dorsal raphe (DR) during exploratory behaviour. In this case, recording started while the rat was actively exploring a lighted cage; at about mid-record the rat gradually ceased exploring, as attested by the decrease in head movement and a change in the pattern of local field potentials (Fig. 3). Exploratory activity resumed around 52 s due to sudden room darkening when the lights were switched off. Using the same analysis parameters (α and segmentation) as before one can see predominant information flow from CA1 to A3 in both exploratory periods. The period of inactivity was characterised by large fluctuations in the resulting directions of information flow using Granger's test (Fig. 4(d)) as opposed to qualitative conclusions one might draw from directed coherence alone where CA1 seems to have a sustained effect on A3 (Fig. 4(a)).

4. Discussion and Future Perspectives

Electrophysiologically one can distinguish four basic types of neural signals: (a) local depolarising and hyperpolarising synaptic potentials, (b) sequences of action potentials (spikes) generated by single neuron firing; (c) local field potentials recorded within some brain structure and which represent averages of the firing of many neurons; and (d) the EEG (electroencephalogram) the resulting residual electric field on the scalp.

In the last few years, mostly in connection with EEG processing, we have seen the growth of proponents of 'modified' coherence methods [21,22, 25–27] much like the one reviewed above. At least in neurobiological circles, in contrast to what happens in econometrics, very little has yet appeared in the specialised literature regarding objective causality tests. This, together with the lack of widespread signal processing expertise among most neuroscientists, and perhaps also due to the possibility of using radical invasive approaches (neural tissue lesion), has contributed to the restricted popularity

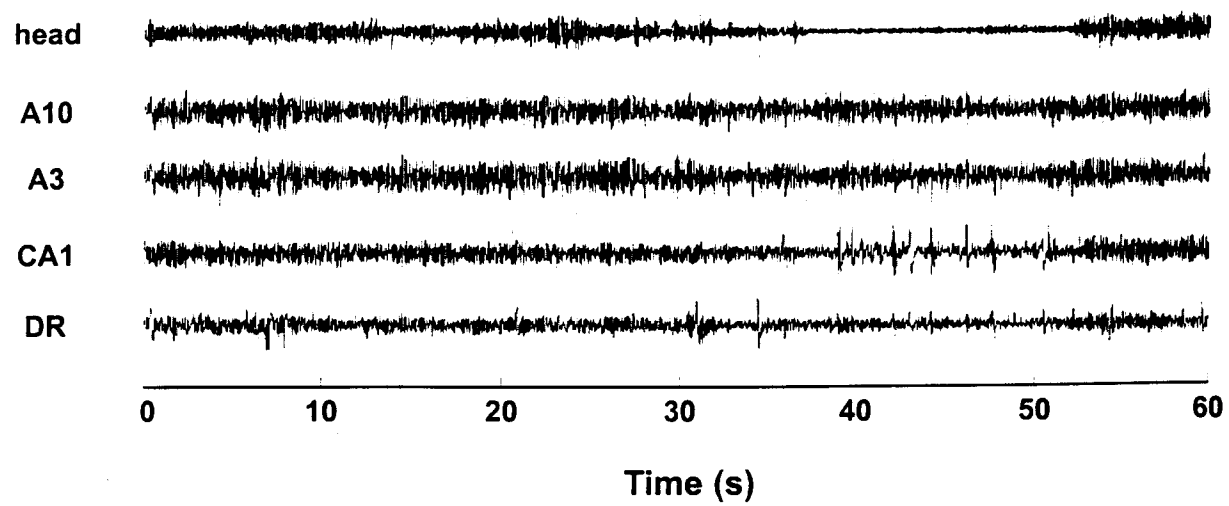

Fig. 3. Local potential field recordings sampled at 256 Hz of an active rat's hippocampal area CA1 and cortical areas A3 and A10 plus the dorsal raphe (DR) together with the simultaneous electromyograms from neck muscles (head movements).

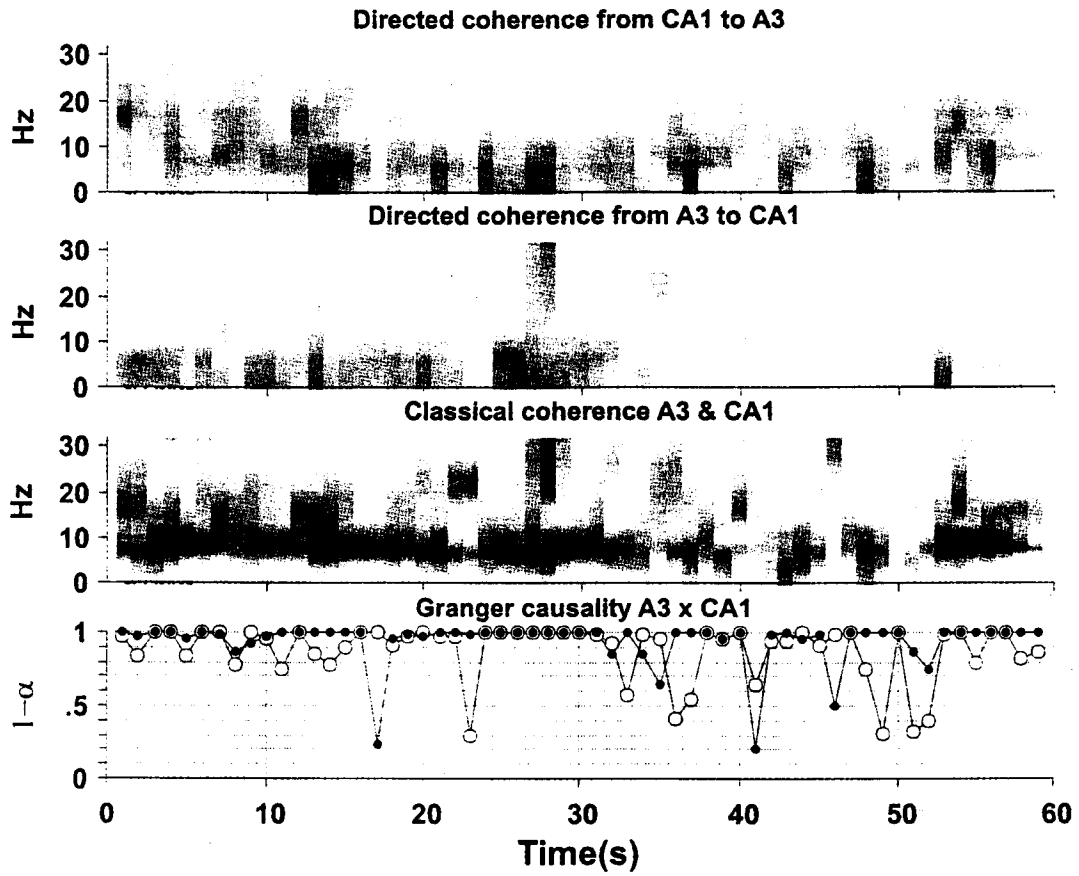

Fig. 4. Comparison of the time–frequency evolution of the directed coherences (**a**) and (**b**) between CA1 and A3 from Fig. 3 with the corresponding classical coherence (**c**). Figure 2**d** displays the corresponding results of the Granger causality test in terms of the lower probability tail $1-\alpha$ of the value of the statistic Λ (see Appendix) for each 2 s signal segment used in the computations through joint VAR modelling of all ($N = 4$) brain signals in Fig. 3. The symbol ● represents the result of the effect of CA1 on A3, while stands for the opposite direction.

of the present methodology despite its clear and superior benefits over classical coherence analysis. It is to fill this gap that we propose the use of the Granger causality test in conjunction with directed coherence, as the latter method provides invaluable visual cues to many issues of interest to neurobiologists, such as frequency of oscillation and so on. Furthermore the Granger causality test, as described here, allows working with multivariate signal traces of single measurements rather than with the ensemble measurements required for statistical inference through variants of directed coherence alone [26].

One of the biggest challenges in neurobiological signal processing today is in the area of action potential processing. Advanced data acquisition systems [28, 29] are now able to record an ever-growing number of single neurons simultaneously (tens of channels) with few existing methods to aid the researcher in combing through for regularities in the resulting overwhelming mass of data. Use of directed coherence seems promising in this kind of analysis [8], especially if coupled with rigourous causality tests.

A number of challenges remain. In experimental setups involving behaving animals neural signals are rather nonstationary, which can make estimation of Eq. (15) difficult, especially with regard to reliable model order p estimates. Also because the neuron, the very unit of brain processing, is a nonlinear element, questions arise as to the generalisation of these ideas to nonlinear prediction models. A further matter of concern to the signal processing community is the issue of faster directed coherence and Granger test calculations.

In summary, joining the frequency information from the directed coherence approach and overcoming its main deficiency regarding objective causality inference through specific tests, the present approach offers a live picture of how brain areas interact that emphasises a shift from structure co-activation – the only picture that conventional

coherence analysis can provide – to the new approach of looking into the mutual effect of the activation of information pathways in the functioning brain.

Acknowledgement. Financial support was provided by PRONEX 41.96.0925.00, CNPq, FAPESP 91/510-8 and FAPESP 96/12118-9.

References

1. Borisyuk G, Borysiuk R, Kirillov A, Kovalenko E, Kryukov V. A new statistical method for identifying interconnections between neuronal networks. Biol Cybern 1985; 52: 301–306
2. Melssen WJ, Epping WJM. Detection and estimation of neural connectivity based on cross correlation. Biol Cybern 1987; 57: 403–414
3. Toyama K, Kimura M, Tanaka K. Cross-correlation analysis of interneuronal connectivity in cat visual cortex. J Neurophysiol 1981; 46: 191–201
4. Eggermont JJ, Johanessman PIM, Aertsen MHJ. Reverse-correlation methods in audiotory research. Q Rev Biophys 1983; 16: 341–414
5. Granger CWJ. Investigating causal relations by econometric models and cross-spectral methods. Econometrica 1969; 37: 424–438
6. Geweke J. Inference and causality in economic time series. In: Griliches Z, Intrilligator MD (eds). Handbook of econometrics. Elsevier, Amsterdam, 1984, pp 1101–1144
7. Lutkepohl H. Introduction to multiple time series analysis. 2nd edn. Springer-Verlag, Berlin 1993
8. Baccala LA, Sameshima K. Directed coherence: a tool for exploring functional interactions among brain structures. In: Nicolelis MAL (ed). Methods for neural ensemble recordings. CRC Press, Boca Raton 1998, pp 179–192
9. Caines P, Chan C. Feedback between stationary stochastic processes. IEEE Trans Autom Contr 1975; AC-20: 498–508
10. Priestley MB. Spectral analysis and time series. Academic Press, London, 1981
11. Schnider SM, Kwong RH, Lenz FA, Kwan HC. Detection of feedback in the central nervous system using system identification techniques. Biol Cybern 1989; 60: 203–212
12. Gevers MR, Anderson BDO. Representation of jointly stationary stochastic feedback processes. Int J Contr 1981; 33: 777–809
13. Gevers MR, Anderson BDO. On jointly stationary feedback-free stochastic processes. IEEE Trans Autom Contr 1982; AC-27: 431–436
14. Marple Jr. SL. Digital spectral analysis. Prentice Hall, Englewood Cliffs, 1987
15. Kay SM. Modern spectral estimation. Prentice Hall, Englewood Cliffs, 1988
16. Haykin S, Kesler S. Prediction error filtering and maximum entropy spectral estimation. In: Haykin S (ed). Nonlinear methods of spectral analysis, Springer-Verlag, Berlin 1979
17. Whittle P. On fitting of multivariable autoregressions and the approximate canonical factorization of a spectral density matrix. Biometrika 1963; 50: 129–134
18. Geweke J, Meese R, Dent W. Comparative tests of causality in temporal systems. J Econometr 1983; 21: 161–194
19. Saito Y, Harashima H. Tracking of information within multichannel EEG record-causal analysis of EEG. In: Yamaguchi N, Fujisawa K (eds). Recent advances in EEG and EMG data processing. Elsevier, Amsterdam, 1981, pp. 133–146
20. Geweke J. Measurement of linear dependence and feedback between multiple time series. J Am Statist Assoc 1982; 77(378): 304–324
21. Kaminski MJ, Blinowska KJ. A new method of the description of the information flow in the brain structures. Biol Cybern 1991: 65: 203–210
22. Franaszczuk PJ, Bergey GK, Kaminski MJ. Analysis of mesial temporal seizure onset and propagation using the directed transfer function method. Electroenceph Clin Neurophysiol 1994; 91: 413–427
23. Krieg W. Connections of the cerebral cortex. I. The albino rat. A topography of the cortical areas. J Comp Neurol 1946; 84: 221–275
24. Shepherd GM (ed). The synaptic organization of the brain, 3rd edn. Oxford University Press, New York, 1990
25. Franaszczuk PJ, Blinowska KJ, Kowalczyk M. The application of parametric multichannel spectral estimates in the study of electrical brain activity. Biol Cybern 1985; 51: 239–247
26. Korzeniewska A, Kasicki S, Kaminski M, Blinowska KJ. Information flow between hippocampus and related structures during various types of rat's behavior. J Neurosci Meth 1997; 73: 49–60
27. Kaminski M, Blinowska K, Szelenberger W. Topographic analysis of coherence and propagation of EEG activity during sleep and wakefulness. Electroenceph Clin Neurophysiol 1997; 102: 216–227
28. Sameshima K, Baccalá LA. Trends in multichannel neural ensemble recording instrumentation. In: Nicolelis MAL (ed). Methods for neural ensemble recordings. CRC Press, Boca Raton 1998, pp 47–60
29. Nicolelis MAL, Ghazanfar AA, Faggin BM, Votaw S, Oliveira LMO. Reconstructing the engram: simultaneous, multisite, many single neuron recordings. Neuron 1997; 18: 520–537.

Appendix. Granger Causality Test Details

For ease of reference, we restate the Granger causality test from j to i described in [7]. The constraint imposed by $a_{ij}(k) = 0$ may be summarised as the null hypothesis:

$$H_0 : \mathbf{Ca} = 0 \tag{A1}$$

where $\mathbf{a}$ is the vector produced by column stacking

$$[\mathbf{A}_1 \ldots \mathbf{A}_p] \tag{A2}$$

and C is a matrix with zero entries except for the factors multiplying $a_{ij}(k)$. Let c be the number of equations represented by Eq. (A1).

The test proceeds by rejecting H_0 (absence of causality) if the statistic

$$\lambda_w = \mathbf{a}\mathbf{C}^T(\mathbf{C}(\mathbf{G}^{-1}\otimes\hat{\mathbf{\Sigma}})\mathbf{C}^T)^{-1}\mathbf{C}\mathbf{a} \qquad \text{(A3)}$$

exceeds the threshold $\chi^2_{\alpha,c}$ (c degrees of freedom) at a significance level α, where

$$\mathbf{G} = \sum_k \tilde{\mathbf{y}}(k)\tilde{\mathbf{y}}(k)^T \qquad \text{(A4)}$$

with $\tilde{\mathbf{y}}(k) = [\mathbf{y}(1)^T \ldots \mathbf{y}(p)^T]^T$ for $\mathbf{y}(k) = [y_1(k) \ldots y_N(k)]^T$, so that k spans all available vector data samples and where $\otimes$ is the Kronecker matrix product and $\hat{\mathbf{\Sigma}}$ a consistent estimator of $\mathbf{\Sigma}$. For easier visualisation, Figs 2 and 4 contain the plots of $1-\alpha$ rather than a plot of the value of λ_w scaled by $\chi^2_{\alpha,c}$.